Detection of Infected Figs by Real-Time Hyperspectral Trasmittance Images

Yusuf Erkan Görgülü[a,*], Habil Kalkan[a], Kadim Taşdemir[b]

[a] Department of Computer Engineering, Süleyman Demirel University, Isparta, 32260, Turkey

[b] Department of Computer Engineering, Antalya International University, Antalya, 07190, Turkey

* Corresponding author Email: yusufgorgulu@sdu.edu.tr

Abstract

Hyperspectral imaging has been used in a wide variety of applications including remote sensing, food safety, food quality, and sorting of different materials. Almost all of these applications depend on reflectance based data acquisition. Reflectance based hyperspectral imaging has its own benefits such as detection of defects on the surface of food commodities, which were caused by mechanical injuries, chemical degradation or fungal contamination. However, the internal structure of these items cannot be clearly identified using hyperspectral reflectance imaging. In this study, a hyperspectral transmittance imaging system is proposed to detect internally contaminated food items non-invasively. The system is designed on a grid based conveyor belt to get transmittance signals in real-time. 2x250W halogen light bulbs are used to illuminate the objects, positioned under the conveyor belt. Images are acquired by a line-scan hyperspectral camera with a spectrum range of 400-1000 nm. The developed system is tested on detecting ***Aspergillus niger*** contaminated dried figs. Using the transmittance signals, an automated classification system is developed. For classification, datasets of 240 dried figs and their flattened counter parts are used. Feature selection is done by forward feature selection up to 30 features. The features are classified by linear discriminant, logistic linear, support vector machine and discriminative restricted Boltzmann machine classifiers. Based on classification performed by 2 times 2 fold cross-validation, the best result is obtained by linear discriminant classifier with 98.75% accuracy using only the best 6 features.

Keywords: Hyperspectral imaging, transmittance, food safety, classification

1. Introduction

In recent decades, food safety has become one of the major aspects of import/export policies between countries. Since most food commodities are subject to mold infection, screening of these items is inevitable. Turkey, being the largest producer of dried figs across the world, is also subject to regulate this process. Most of the dried fig cooperatives in Aegean region of Turkey have been using a manual screening procedure to identify black mold (***Aspergillus niger***, ***A.niger***) contamination in their products. In this procedure workers use a nail-like object, which they insert deep into the dried fig from the ostiole (fig fruits opening) to grab inner constituents. Then the ejected nail is visually inspected whether it contains any sign of black mold. This procedure is invasive and potentially harmful since the procedure involves using the same nail for all dried figs. Thus, any remaining strain of black mold may propagate to uncontaminated products. Another drawback of this evaluation is caused by the subjective decision given by the observer. If the observer is not experienced enough, the risk of misdetection grows.

Hyperspectral imaging systems (HSI) have been used as an alternative to manual inspection in the past decades, due to the fact that they have the advantage of non-invasive screening of food commodities. HSI systems may utilize reflectance, transmittance or absorbance properties of materials under inspection or combinations of these. Huang et al. (2013) used transmittance mode images of vegetable soybeans to detect damage caused by insects. The spectra of 400 to 1000 nm was used to extract four statistical features and 95.6% overall accuracy was achieved. Lu and Ariana (2013) used both reflectance (450-740 nm) and transmittance (740-1000 nm) images of pickling cucumbers to detect fruit fly infestation and outer performed manual inspection by achieving 82% to 88% accuracy rates for reflectance, and 88% to 93% accuracies for transmittance. Yoon et al. (2008) also used both reflectance and transmittance to detect bone fragments embedded in chicken fillets. In their study, transmittance images were used to enhance the location of the bone fragment and then both modes of images were fused. They achieved 100% accuracy with a 10% false positive rate. Coelho et al. (2013) used transmittance images to detect a parasite related with the clam (***Mulinia edulis***). They identified that 600-950 nm spectra was essential to detect the parasite. Based on a classification rule using Mahalanobis distance, they achieved 100% accuracy identifying the parasite with full spectra. Leiva-Valenzula et al. (2015) assessed the internal quality of blueberries using both transmittance and reflectance images between 400 nm and 1000 nm. They used regression (partial least squares (PLS) and interval PLS) techniques to sort and grade blueberries rather than classification techniques. They used these techniques to calibrate two parameters: firmness index and soluble solids content. Ochoa et al. (2016) used reflectance images of banana tree leaf blade to detect Black Sigatoka, a disease caused by ***Mycosphaerella fijiensis***. They designed an HSI system particularly to image banana leaves at VIS-NIR spectra using a CCD camera and an optical spectrograph. In this paper they mostly focused on settings of HSI system. In a former study of ours (Ortaç et al., 2015), we investigated reflectance properties of dried fig images to classify black mold infected figs.

Among the spectra of 400 nm to 1000 nm we only used 50 prominent bands to accurately classify dried fig as sound or contaminated. Using only 5 bands out of 50, an accuracy rate of 100% was achieved. There also exist some other studies that harness hyperspectral imaging for abiotic materials. Serranti et al. (2015) used hyperspectral imaging to classify demolition waste materials. They utilized the spectra of 1000-1700 nm with 6 different materials for classification. Picón et al. (2012) used reflectance images of waste of electric an electronic equipment (WEEE) components to distinguish non-ferrous materials like copper, steel, aluminum, brass. They decorrelated hyperspectral data using fuzzy-logic and they extracted features from spatial and spectral data, since adjacent band values do not change rapidly. Their classification accuracy was above 96%. These studies suggest that HSI systems are adequate to identify either biologic or abiotic materials with high accuracies.

In this study, a hyperspectral transmittance imaging system is proposed to detect internally contaminated food items automatically. A spectral range of 400-1000 nm with 784 different spectral bands has been used. The system is tested by using dried figs with two classes (sound figs and ***A. niger*** contaminated ones). Two different datasets (one from dried figs in natural form and one from their flattened version) are obtained for experimental evaluation. Features are calculated as the mean intensity values and standard deviations of each spectral band image. However, for a real-time operational system, the best 30 features are determined by forward feature selection based on Jeffreys-Matusita distance, instead of using all features. The selected features are then classified by five different classifiers in two times two fold cross-validation scheme. The system is explained in Section 2, the experimental results are given in Section 3, and conclusions are in Section 4.

2. Materials and Methods

2.1. Materials

A total of 280 dried fig samples are obtained from TARİŞ Fig Cooperative Union who processes the dried figs in Aegean region of Turkey. The figs are manually labeled by experts into sound and ***A***. ***niger*** positive classes by visual examination. The figs which do not have black mold indication at the outer surface have been checked by using nails. Experts use nails to take some samples from the inner part of figs to seek the black mold contamination. Among the 280 samples, 120 of them are sound and the remaining 160 samples are ***A.niger*** contaminated.

2.2. Methods

In order to obtain transmittance images of dried figs, a conveyor with a metal grid belt is used. The imaging system includes a grid conveyor belt, light sources, light focusing optics, Specim PFD-C-XX-V10 hyperspectral camera, and a dark room for housing the camera. Figure 1 illustrates the designed HSI system.

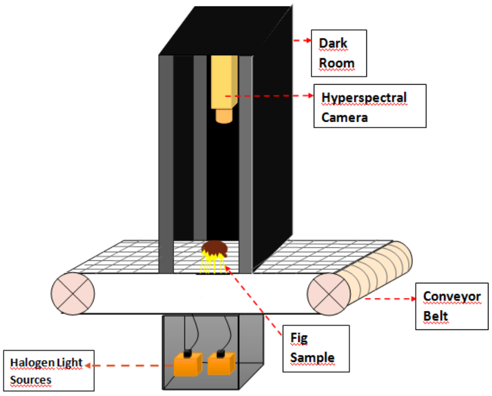

Figure 1.The designed HSI system.

The gaps existing in the grid belt allow lights to penetrate through the samples and reach to the hyperspectral camera positioned above the samples. As illumination source, two 250 Watt halogen light bulbs, which are positioned below the metal grid belt targeting to the hyperspectral camera, are used. Above the metal belt, an aperture is used to suppress excess light to avoid saturation of the camera sensor. The lights generated at halogen bulbs are directed to the aperture by using focusing optics. Using the hyperspectral camera, it is possible to obtain images of a spectra ranging from 400nm to 1000nm. Raw images are obtained on the conveyor belt at a speed of 0.6 rpm (rotations per minute).

Initially, the dried figs are imaged as in natural dried form (Figure 2). Then the dried figs are pressed to have flattened shape (Figure 3). The flattening process is used to obtain figs samples at standard thickness. The flattened figs are then imaged. As a result, we obtain two different hyperspectral datasets obtained from natural and flattened figs.

Figure 2. Contaminated (A and B) , uncontaminated (C and D) dried figs in natural form.

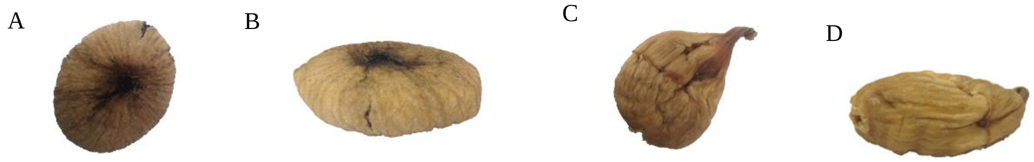

Figure 3. Contaminated (A and B) , uncontaminated (C and D) dried figs in flattened form.

Before imaging the fig samples, white and black calibration images ($W^s(x,y)$ and $D^s(x,y)$) are obtained for each spectral band, s, individually. The black calibration image, $D^s(x,y)$, is the image acquired at spectral band s by turning the light sources off and by closing the camera lens. In contrast, the white calibration image, $W^s(x,y)$, is the image obtained by turning the lights on and imaging a white plain paper on conveyor belt. Using these calibration images, the raw image,$I^s(x,y)$, is calibrated as in Eq(1) (Sun, 2010):

$$I_C^S(x,y) = \frac{I^S(x,y) - D^S(x,y)}{W^S(x,y) - D^S(x,y)} \cdot 100 \tag{1}$$

where $I_c^s(x,y)$ and $I^s(x,y)$ are the calibrated and the raw image acquired at the s^{th} spectral band, respectively. The calibrated images are then masked using the spectral images where the object of interest (ROI) can be identified clearly. The best images where the background can be easily separated from ROI are usually observed at near-infrared bands (around 850 nm). The image at 850 nm is hence used for generating a mask for ROI extraction by a simple thresholding. However, we observe light leakage through the borders of figs at spectral bands lower than 710 nm and these light leakage cause saturation in imaging sensors. Therefore the mask generated at 850 nm is narrowed for extracting the ROI at visible regions (lower than 710 nm). Each spectral image, $I_i^s(x,y)$, is then transformed into feature space $F_i^s = \{\mu_i^s, \sigma_i^s\} \in R^2$ by evaluating the mean intensity μ_i^s and standard deviation (σ_i^s) represented in Eq. (2) and Eq. (3), respectively:

$$\mu_i^S = \frac{1}{n}\sum_{j=1}^{n} I_i^S(x,y) \tag{2}$$

$$\sigma_i^S = \sqrt{\frac{1}{n-1}\sum_{j=1}^{n}(I_i^S(x,y) - \mu_i^S)^2} \tag{3}$$

where superscript s indicates the spectral band and subscript i indicates the sample number, respectively. Then, the features of spectral images are combined to represent a fig sample in feature space $F_i = \{F_i^s\} \in R^{2t}, s = 1,2,\cdots,t$ where t is the number of spectral bands in hyperspectral images.

The features in hyperspectral images may be correlated to each other, especially in adjacent bands, and the use of correlated features decreases the classification accuracy. Therefore, the features are selected by forward feature selection based on the Jeffreys-Matusita distances, D_{JM}(Bruzzone and Serpico, 2000):

$$D_{JM} = \sqrt{2 \cdot (1 - e^{(-D_B)})} \tag{4}$$

The Jeffreys-Matusita distance in Eq.(4) is a special form of Bhattacharya distance Eq.(5), D_B:

$$D_B = \frac{1}{8}(\mu_1 - \mu_2)^T \Sigma^{-1} (\mu_1 - \mu_2) + \frac{1}{2} \ln\left(\frac{\det\Sigma}{\sqrt{\det\Sigma_1 \det\Sigma_2}}\right) \quad (5)$$

$$\text{where}, \Sigma = \frac{\Sigma_1 + \Sigma_2}{2}$$

where μ_j and Σ_j are the mean vector and covariance matrix of the feature vectors of j^{th} class, respectively. The selected features are then applied to various classifiers in a 2 times 2 fold cross-validation scheme, including linear classifier (LDC), quadratic linear classifier (QDC), logistic linear classifier (LOGLC), support vector machine classifier with radial basis function kernel (SVM-rbf) and discriminative restricted Boltzmann machine classifier (D-RBM).

3. Results and Discussion

Since the thickness in flattened samples is less than the samples in natural form, the penetration of illumination sources is high relative to the natural samples. Whether the figs are contaminated or uncontaminated, the intensity of transmitted signal is higher at flattened figs compared to natural figs (Figure 2). The spectra from 400 nm to approximately 440 nm correspond to the noisy images, mostly contaminated by salt and pepper noise and thus intensities at this region are ignored. The same noisy structure is also observed at the far end of the spectra, namely 950nm to the utmost wavelength present. This is both valid for natural and flattened samples, most probably caused by camera sensor noise.

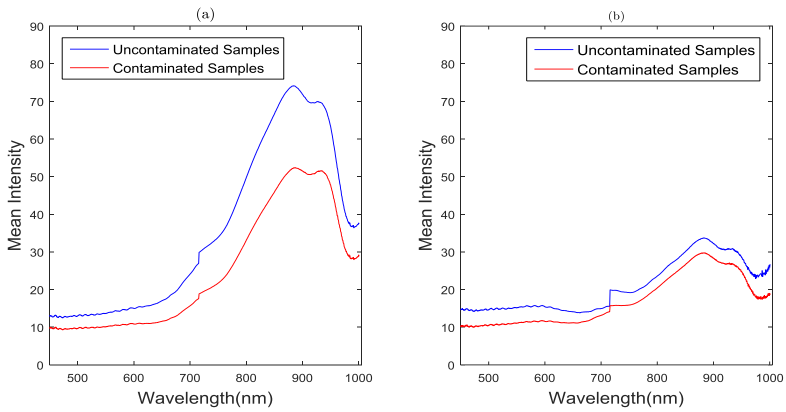

Figure 4. Mean intensity averages for (a) Flattened samples, (b) Natural samples

In Figure 4, there exists a sharp jump at about 710nm, which is more obvious in Figure 4-b’s uncontaminated samples. This jump is caused by the transition between different masks used in masking process. The visual distance between two classes is clearly recognizable. The Bhattacharya distance and the Jeffreys-Matusita distance of both flattened and natural samples with respect to their feature sets are given in Figure 5 and Figure 6, respectively. Distances are calculated using a set of features including only one feature up to a set including thirty features. These features are obtained by feed-forward feature selection based on Jeffreys-Matusita distance. Both distance related figures (Figure 5 and Figure 6) show that natural samples have a higher distance almost with every feature set size, except at the very beginning.

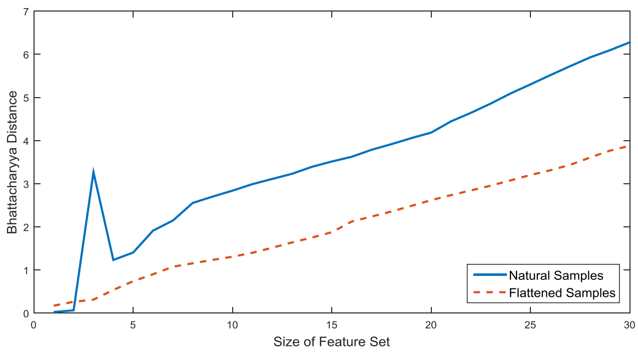

Figure 5. Bhattcharya distances of natural and flattened samples with respect to feature set size.

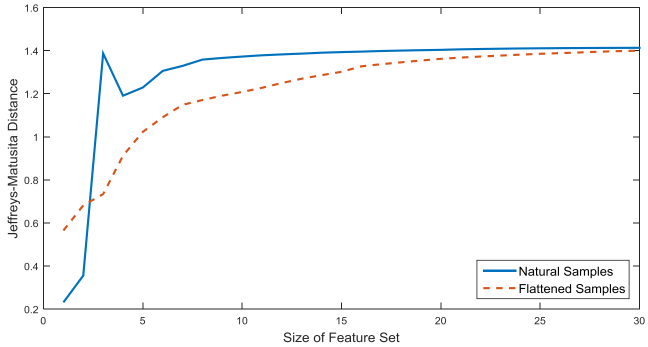

Figure 6. Jeffreys-Matusita distances of natural and flattened samples with respect to feature set size.

The features are ranked using feed-forward feature selection criteria considering the distances of the selected subset and the classification is performed at each feature subset. The classification accuracy is evaluated by two times two fold cross validation in that the presented accuracies are the mean of four trials obtained from these validations. The classification procedures are performed with five different classifiers and the accuracies obtained at different feature sizes are presented at Figure 7 and Figure 8 for flattened and natural fig datasets. It is observed from Figure 7 and Figure 8 that, Logistic, Linear and Quadratic classifiers outperform the other SVM-rbf and D-Rbm classifiers in terms of classification accuracy. The 2 times 2 fold cross-validation classification results for flattened figs and for natural figs are shown in Figure 7 and Figure 8. Classification results agree with distance figures given in Figure 5 and Figure 6. In both classification accuracy figures in Figure 7 and Figure 8, classifiers of natural samples are more accurate than their flattened counterparts.

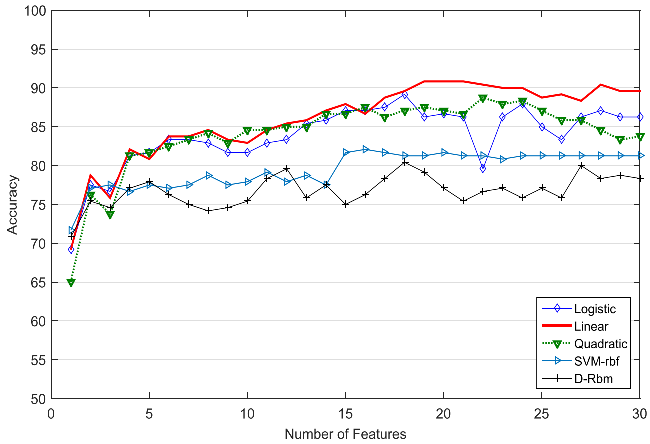

Figure 7. Classification accuracies regarding number of features, (Flattened samples).

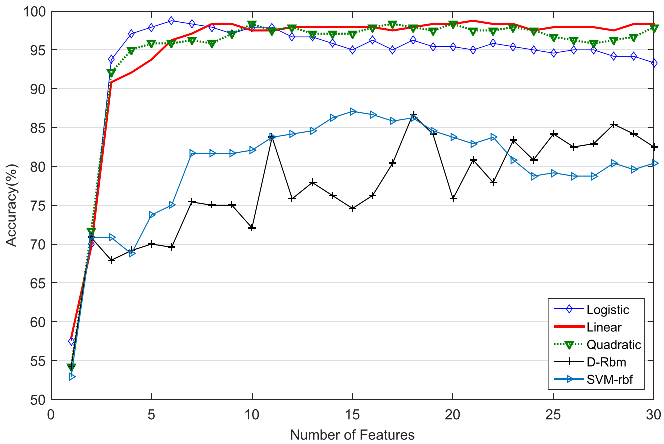

Figure 8.Classification accuracies regarding number of features, (Natural samples).

For flattened samples (Figure 7), linear classifier using 19 features has the highest accuracy of 90.83% among others. Natural samples' classification results (Figure 8) have the highest accuracy rate of 98.75% for logistic linear classifier with 6 features.

4. Conclusions

Food commodities with adequate level of water are prone to mold infection under environmental conditions. Even dried foods are under this risk. These sort of problems pose a great threat for most of the agricultural commodities. Disadvantages of conventional food assessment methods suggest solutions that empower novel computer vision systems. In this study an agricultural commodity; dried fig is determined whether it is contaminated with ***A.niger*** mold using hyperspectral transmittance approach. To detect contaminated dried figs, we use transmittance properties among specified wavelengths. Results indicate that for flattened samples LDC is superior to other classifiers, with a 90.83% and for the normal samples same results are valid for LOGLC with 98.75% accuracy. These experimental results suggest that this method may successfully be applied not only to dried figs but also for the most of the agricultural commodities.

This study also gives us insight to build a real-time system. As a further improvement for the proposed system, illumination sources will be replaced by relatively low power consuming infrared (IR) light emitting diodes (LED) at 850 nm peak wavelength since high power consumption and high heat dissipation are the drawbacks of halogen light sources. This change will also result in narrowing the dataset to the specified wavelengths of IR LED which eases computation.

Acknowledgements

This work has been supported by the Scientific and Technological Research Council of Turkey (TUBITAK, Grant no.113O878 and no.113O879).

References

Bruzzone, L., and S. B. Serpico, 2000. A technique for feature selection in multiclass problems. *International Journal of Remote Sensing,* 21 (3), 549-563.http://dx.doi.org/10.1080/014311600210740

Coelho, P. A., M. E. Soto, S. N. Torres, D. G. Sbarbaro and J. E. Pezoa, 2013. Hyperspectral transmittance imaging of the shell-free cooked clam Mulinia edulis for parasite detection. *Journal of Food Engineering,* 117 (3), 408-416.http://dx.doi.org/10.1016/j.jfoodeng.2013.01.047

Huang, M., X. Wan, M. Zhang and Q. Zhu, 2013. Detection of insect-damaged vegetable soybeans using hyperspectral transmittance image. *Journal of Food Engineering,* 116 (1), 45-49.http://dx.doi.org/10.1016/j.jfoodeng.2012.11.014

Leiva-Valenzuela, G. A., R. Lu and J. M. Aguilera, 2014. Assessment of internal quality of blueberries using hyperspectral transmittance and reflectance images with whole spectra or selected wavelengths. *Innovative Food Science & Emerging Technologies,* 24, 2-13.http://dx.doi.org/10.1016/j.ifset.2014.02.006

Lu, R. and D. P. Ariana, 2013. Detection of fruit fly infestation in pickling cucumbers using a hyperspectral reflectance/transmittance imaging system. *Postharvest Biology and Technology,* 81, 44-50.http://dx.doi.org/10.1016/j.postharvbio.2013.02.003

Ochoa, D., J. Cevallo, G. Vargas, R. Criollo, D. Romero, R. Castro and O. Bayona, 2016. Hyperspectral imaging system for disease scanning on banana plants. *Proc. SPIE 9864, Sensing for Agriculture and Food Quality and Safety VIII*, (s. 98640M). http://dx.doi.org/10.1117/12.2224242

Ortaç, G., A. S. Bilgi, Y. E. Görgülü, A. Güneş, H. Kalkan and K. Taşdemir, 2015. Classification of black mold contaminated figs by hyperspectral imaging. In *2015 IEEE International Symposium on Signal Processing and Information Technology (ISSPIT)*, 227-230. Abu Dhabi, 7-10 December.http://dx.doi.org/10.1109/ISSPIT.2015.7394332

Picón, A., O. Ghita, A. Bereciartua, J. Echazarra, P. F. Whelan, and P. M. Iriondo, 2012. Real-time hyperspectral processing for automatic nonferrous material sorting. *Journal of Electronic Imaging, 21* (1), s. 013018-1-013018-9.http://dx.doi.org/10.1117/1.JEI.21.1.013018

Serranti, S., R. Palmieri and G. Bonifazi, 2015. Hyperspectral imaging applied to demolition waste recycling: innovative approach for product quality control. *Journal of Electronic Imaging,* 24 (4), 043003.http://dx.doi.org/10.1117/1.JEI.24.4.043003

Sun, D. W., 2010. Hyperspectral Imaging for Food Quality Analysis and Control, ch. 1, 36 p, San Diego: Academic Press.

Yoon, S. C., K. C. Lawrence, D. P. Smith, B. Park and W. R. Windham, 2008. Embedded bone fragment detection in chicken fillets using transmittance image enhancement and hyperspectral reflectance imaging. *Sensing and Instrumentation for Food Quality and Safety,* 2 (3), 197-207.http://dx.doi.org/10.1007/s11694-008-9044-2